



## RESEARCH LETTER

10.1029/2023GL103025

### Key Points:

- Relative to the simulated future state with reduced El Niño–Southern Oscillation (ENSO) variability, Atlantic Meridional Overturning Circulation (AMOC) slowdown strengthens ENSO by amplifying Ekman upwelling feedback
- AMOC slowdown facilitates the occurrence of Central Pacific El Niño events
- AMOC impacts on ENSO are smaller than model internal variability during the twenty-first century

### Supporting Information:

Supporting Information may be found in the online version of this article.

### Correspondence to:

W. Liu,  
wei.liu@ucr.edu

### Citation:

Liu, W., Duarte Cavalcante Pinto, D., Fedorov, A., & Zhu, J. (2023). The impacts of a weakened Atlantic Meridional Overturning Circulation on ENSO in a warmer climate. *Geophysical Research Letters*, 50, e2023GL103025. <https://doi.org/10.1029/2023GL103025>

Received 26 JAN 2023

Accepted 6 APR 2023

# The Impacts of a Weakened Atlantic Meridional Overturning Circulation on ENSO in a Warmer Climate

Wei Liu<sup>1</sup> , David Duarte Cavalcante Pinto<sup>1</sup>, Alexey Fedorov<sup>2,3</sup> , and Jiang Zhu<sup>4</sup>

<sup>1</sup>Department of Earth and Planetary Sciences, University of California Riverside, Riverside, CA, USA, <sup>2</sup>Department of Earth and Planetary Sciences, Yale University, New Haven, CT, USA, <sup>3</sup>LOCEAN/IPSL, Sorbonne University, Paris, France, <sup>4</sup>Climate and Global Dynamics Laboratory, National Center for Atmospheric Research, Boulder, CO, USA

**Abstract** This study quantifies the impacts of the Atlantic Meridional Overturning Circulation (AMOC) on the El Niño–Southern Oscillation (ENSO) under anthropogenic warming by comparing climate change model simulations with declining and fixed strengths of the overturning. After the 1980s, a weakened AMOC is shown to reduce the strength of the annual cycle of sea surface temperature (SST) in the eastern equatorial Pacific and induce anomalous cross-equatorial northerly winds there, which strengthens ENSO variability by about 11%. An analysis of the Bjerknes stability index reveals that this intensification of ENSO results mainly from enhanced Ekman upwelling feedback due to amplified atmospheric wind response to SST anomalies and oceanic upwelling response to equatorial wind stress anomalies. The weakened AMOC also promotes the occurrence of Central Pacific El Niño events and reduces ENSO skewness. These AMOC impacts on ENSO magnitude and complexity throughout the twenty-first century are however smaller than ENSO variations expected from internal climate variability.

**Plain Language Summary** Here, we use climate model simulations to study how changes in the Atlantic Meridional Overturning Circulation (AMOC) influence the El Niño–Southern Oscillation (ENSO) in a warming climate. We find that the overturning circulation slowdown caused by global warming can strengthen the ENSO variability by about 11% over 1981–2100 by reducing the annual cycle of sea surface temperature and cross-equatorial winds in the eastern equatorial Pacific. The detailed physical mechanism explaining this ENSO intensification involves changes in ocean-atmosphere feedback. We also find that the declining AMOC makes El Niño events with the Central Pacific temperature pattern more frequent. The above effects of the AMOC on ENSO are however smaller than differences expected from model internal climate variability.

## 1. Introduction

The Atlantic Meridional Overturning Circulation (AMOC) plays a crucial role in Earth's climate (Bryden & Imaewaki, 2001; W. Liu et al., 2017). This ocean circulation system has been observed to slow down over the past two decades as measured by the RAPID array at 26.5°N in the North Atlantic (Frajka-Williams, 2015; Smeed et al., 2018); however, given the relatively short observational period, this AMOC slowdown can be part of natural climate variability (Robert et al., 2014). According to some proxy reconstructions, the AMOC slowdown might have started as early as in the middle-to-late twentieth century (Caesar et al., 2021, 2018; Rahmstorf et al., 2015; Thornalley et al., 2018); this conclusion however has been debated (Kilbourne et al., 2022). During the twenty-first century, the AMOC is projected to continue to decline as summarized by the Fifth Assessment Report of the Intergovernmental Panel on Climate Change (IPCC AR5). For example, under the RCP8.5 (Representative Concentration Pathway 8.5) global warming scenario, the AMOC strength will decrease by 12%–54% by 2100. In the recent IPCC AR6, the AMOC also shows a comparable decline by 2100 under a similar climate scenario of the SSP585 (an updated version of RCP8.5 but now based on Shared Socioeconomic Pathways, cf., Weijer et al., 2020), although the newer models put the starting time of the AMOC decline by about one decade later due to a stronger anthropogenic aerosol forcing used (Hassan et al., 2021; Menary et al., 2020).

The AMOC slowdown has been shown to impact the global and regional climate (Li & Liu, 2022; W. Liu et al., 2020; Ren & Liu, 2021). For example, in the absence of anthropogenic global warming, a weakened AMOC can remotely cause a meridionally asymmetric change in the mean state in the eastern equatorial Pacific through atmospheric teleconnections and local coupled air-sea feedback (Dong & Sutton, 2002; Zhang & Delworth, 2005), featuring a substantial weakening of sea surface temperature (SST) annual cycle there (Timmermann et al., 2007).

© 2023. The Authors.

This is an open access article under the terms of the [Creative Commons Attribution-NonCommercial-NoDerivs License](#), which permits use and distribution in any medium, provided the original work is properly cited, the use is non-commercial and no modifications or adaptations are made.

and a reduction in mean cross-equatorial winds (Hu & Fedorov, 2018). These changes in the mean state lead in turn to an eastward shift of El Niño–Southern Oscillation (ENSO) SST anomalies, a longer and more regular ENSO period (Willmanson et al., 2018) and an increase in the magnitude of ENSO variability (Dong & Sutton, 2007; Timmermann et al., 2007). Yet a recent study (Orihuela-Pinto et al., 2022) argued that a collapsed AMOC acts to decrease, instead of increase, the ENSO variability.

Most of the above insights of AMOC impacts however are obtained from classical freshwater hosing experiments causing a slowdown or a full collapse of the AMOC. To the best of our knowledge, the impacts of projected AMOC slowdown have not been explicitly assessed in the context of anthropogenic warming via fully coupled climate model experiments. Also, it is well recognized that climate model projections of ENSO intensity have large uncertainties (Cai et al., 2022, 2015; Collins et al., 2010; Stevenson, 2012) because ENSO is controlled by a delicate balance of amplifying and damping feedback, which is modified by climate change simultaneously (Collins et al., 2010; Fedorov et al., 2020; Fedorov & Philander, 2000, 2001; Hu & Fedorov, 2018; Zheng et al., 2016). So far, efforts to understand ENSO projections have mainly focused on local processes in the tropic Pacific, whilst remote effects such as those from the future AMOC slowdown have received less attention. Therefore, it remains unclear how and to what extent the projected AMOC slowdown can affect future ENSO variability during the twenty-first century, which is the focus of the current study.

## 2. Data and Methods

### 2.1. Observations

We use four monthly reconstructed SST data sets to assess historical ENSO variability during 1861–1980. These data sets are COBE-SST2 on a  $1^\circ$  grid (Hirahara et al., 2014), ERSST.v4 (Huang et al., 2015; W. Liu et al., 2015) and ERSSTv5 (Huang et al., 2017) on a two-degree grid and KAPLAN EXTENDED v2 on a five-degree grid (Kaplan et al., 1998). We compute the mean over these four SST data sets as well as one standard deviation. For each data set, we calculate the Niño 3.4 ENSO index by averaging the detrended SST anomalies over the Niño 3.4 area ( $5^\circ\text{N}$ – $5^\circ\text{S}$ ,  $170^\circ\text{W}$ – $120^\circ\text{W}$ ). The mean of the Niño 3.4 index depicts a significant ENSO period at 2–4 yr during 1861–1980 (Figure 1c).

### 2.2. Climate Model Simulations

We employ a broadly used climate model, the Community Climate System Model version 4 (CCSM4) with the standard  $1^\circ$  atmospheric resolution (Deser et al., 2012), which captures well the 2–4 yr periodicity of ENSO, even though with a larger amplitude (Figure 1c), as well as an annual cycle of SST in the eastern equatorial Pacific similar to the observations (Figure S1 in Supporting Information S1). We use five ensemble members of CCSM4 historical and RCP8.5 simulations from 1861 to 2100. Consistent with most of IPCC AR5 model results, CCSM4 simulates a relatively steady AMOC in the early and middle twentieth century (Figure 1a), which is likely due to the compensation between the warming effect of rising greenhouse gases and the cooling effect of growing aerosols at that time (Delworth & Dixon, 2006). The model AMOC weakens after the 1980s when aerosol emissions began to decline over North America and Europe while greenhouse gas concentrations continued to rise.

Utilizing CCSM4 historical and RCP8.5 simulations, we conduct a parallel sensitivity experiment with corresponding five ensemble members, which is branched from the year 1980 of the historical simulation and driven by the same historical and RCP8.5 forcings except that a small amount of freshwater is gradually removed from the surface in the subpolar North Atlantic and uniformly redistributed over rest of the global ocean (details are provided in W. Liu et al., 2020). This experimental setup helps maintain a constant AMOC strength throughout the twenty-first century even under anthropogenic warming (Figure 1a). The AMOC strength is defined as the maximum of the annual mean stream function below 500 m in the North Atlantic. For brevity, we denote the historical simulation over 1861–1980 as “HIST”, and the historical plus RCP8.5 simulation over 1981–2100 as “RCP85” since most of this period falls under the RCP8.5 scenario. We denote the sensitivity experiment for years 1981–2100 as “RCP85\_fxAMOC”, so that the difference between RCP85 and RCP85\_fxAMOC shows the climate impacts of the AMOC slowdown under the chosen global warming scenario. We also test the significance of the difference between these two sets of simulations relative to internal climate variability (Zheng et al., 2019) at 95% confidence level based on the Student’s *t* test between the RCP85 and RCP85\_fxAMOC ensembles. This internal climate variability manifests in the inter-member difference within each ensemble. Accordingly, for each

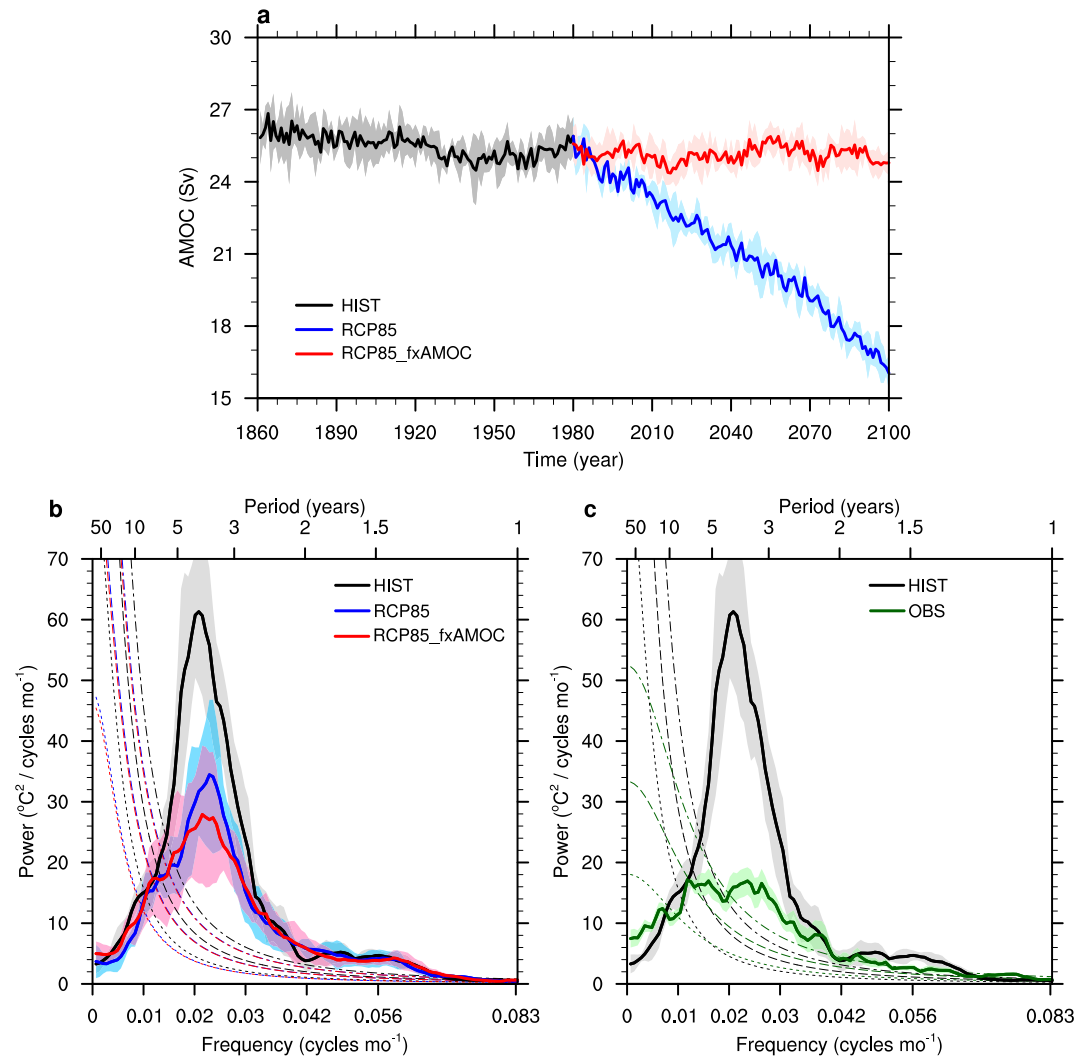


**Figure 1.** (a) Atlantic Meridional Overturning Circulation (AMOC) strength in the HIST simulation for years 1861–1880 (black), RCP85 simulation for 1881–2100 (blue), and RCP85\_fxAMOC simulation for 1881–2100 (red). AMOC strength is defined as the maximum of the annual mean stream function below 500 m in the North Atlantic. (b) Power spectra of the Niño 3.4 indices in the HIST (black), RCP85 (blue), and RCP85\_fxAMOC (red) simulations and associated 95% confidence limits (dashed/dotted curves). (c) Power spectra of the Niño 3.4 indices in the HIST (black) and observations (green) over 1861–1880. In all cases solid lines denote ensemble-mean results, and light color shading indicates ensemble spread.

of the HIST, RCP85, and RCP85\_fxAMOC simulations, we calculate the ensemble mean over five members and the ensemble spread as one standard deviation among ensemble members.

### 3. Results

We first explore the mean-state change in the tropical Pacific between the RCP85 and HIST simulations. The ensemble mean result shows an enhanced equatorial SST warming relative to the subtropics during the twenty-first century (Figure 2a). The equatorial enhanced response (Knutson & Manabe, 1995; Meehl et al., 2000) to anthropogenic forcing is associated with changes in surface latent heat fluxes due to wind speed change, shortwave cloud radiation, and ocean mixing (Z. Liu et al., 2005). A warming maximum emerges at the eastern tropical Pacific and a warming minimum emerges to the south of the equator, accompanied by reduced equatorial easterlies but intensified southeast trade winds off the equator (Figure 2a), which points to the role of the wind-evaporation-SST feedback in shaping this pattern (Xie et al., 2010; Xie & Philander, 1994). The interplay of different mechanisms that lead to the development of this pattern on different timescales and across different models has been discussed

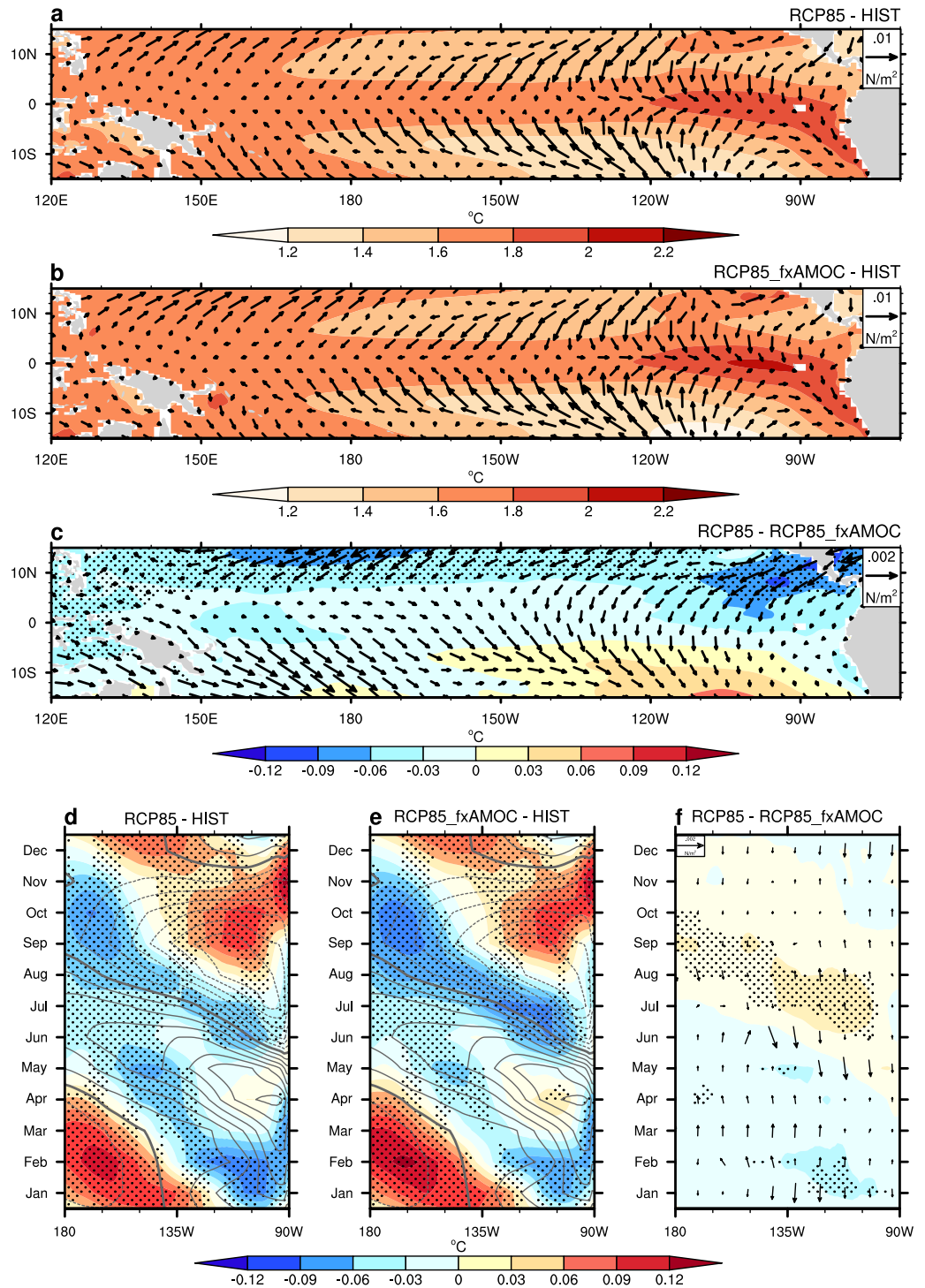


**Figure 2.** (a–c) Ensemble-mean differences of annual mean sea surface temperature (SST) (color shading, in °C) and surface wind stress (vectors, in N/m<sup>2</sup>) between (a) the RCP85 and HIST simulations, (b) RCP85\_fxAMOC and HIST simulations, and (c) RCP85 and RCP85\_fxAMOC simulations. (d–f) Hovmöller diagrams showing ensemble-mean differences for the annual cycle of SST (color shading, in °C) in the tropical Pacific (5°S–5°N) between (d) RCP85 and HIST simulations, (e) RCP85\_fxAMOC and HIST simulations, and (f) RCP85 and RCP85\_fxAMOC simulations. The annual cycle of SST from the HIST simulation (contours in °C with a contour interval of 0.2°C; positive solid, negative dashed and zero contours thickened) is overlaid in panels (d and e). The ensemble-mean difference for the annual cycle of surface wind stress (vectors, in N/m<sup>2</sup>) between RCP85 and RCP85\_fxAMOC simulations is superposed in panel (f). Note the anomalous northerly winds during May–June in panel (f). Stippling in panels (c–f) indicate where SST differences are statistically significant at a 95% confidence level based on Student's *t* test.

in Heede and Fedorov (2021, 2023) and Heede et al. (2020, 2021). The warming maximum and minimum would reach even greater amplitudes without AMOC slowdown (Figure 2b). This is because a weaker Atlantic overturning induces cooling and warming SST anomalies to the north and south of around 3°S, respectively, in the eastern and central Pacific (CP), along with anomalous cross-equatorial northerly winds (Figure 2c).

Changes in ENSO are tied to the resulting change in the mean state of the tropical Pacific (An & Jin, 2000; Fedorov et al., 2020; Fedorov & Philander, 2000, 2001; Jin et al., 2006). The ensemble mean of ENSO variability peaks at 4, 3.64, and 3.87 yr in the HIST, RCP85, and RCP85\_fxAMOC simulations, respectively, meaning that the projected anthropogenic warming shortens future ENSO period while the AMOC slowdown can make the ENSO period even shorter. On the other hand, the ensemble-mean magnitude of ENSO variability decreases over the twenty-first century under the RCP8.5 scenario, and such decrease might be even larger without the projected AMOC slowdown (Figure 1b). This result suggests that, relative to the simulated future state with reduced ENSO variability, a weakened AMOC under global warming acts to amplify ENSO variability, which is consistent with the findings of Dong and Sutton (2007) and Timmermann et al. (2007) but is different from the study of Orihuela-Pinto et al. (2022).

Despite the ensemble-mean result showing ENSO intensification, this AMOC impact is not statistically significant relative to internal climate variability, that is, the inter-member difference within either ensemble. Taking the 4 yr period ENSO variance for example, the variance significantly ( $p = 0.00$ ) decreases by  $-47.2\% \pm 13.8\%$  from the HIST to RCP85 simulation but insignificantly ( $p = 0.39$ ) increases by  $10.6\% \pm 40.5\%$  from the RCP85\_fxAMOC to RCP85 simulation. The latter means that the inter-member difference within the ensembles of either simulation is greater than the ensemble-mean difference between the two global warming simulations. In other words, ENSO variance may actually decrease between a few of the ensemble members from the RCP85\_fxAMOC and RCP85 simulations, respectively.

To investigate the physical mechanisms of the AMOC on modulating future ENSO, we first examine the changes in the SST annual cycle in the eastern equatorial Pacific among the ensemble means of the HIST, RCP85, and RCP85\_fxAMOC simulations. The difference between the RCP85 and HIST simulations reveals a general reduction of the SST annual cycle during the twenty-first century, though it also illustrates some anomalous semi-annual signals (Figure 2d). The difference between the RCP85\_fxAMOC and HIST simulations shows a similar pattern of reduced SST annual cycle but with smaller magnitude of the reduction (Figure 2e), meaning that a weakened AMOC indeed acts to further reduce the SST annual cycle in the eastern equatorial Pacific relative to the simulated future state with an already weakened annual cycle (Figure 2f). This result is consistent with those from Dong and Sutton (2007) and Timmermann et al. (2007), suggesting that a weakened annual cycle can lead to intensification of the ENSO amplitude and vice versa via the frequency entrainment mechanism (Chang et al., 1994; Z. Liu, 2002; Timmermann, Lorenz, An, Clement, & Xie, 2007). We also find that the anomalous cross-equatorial northerly winds are especially strong in May–June (Figure 2f), which indicates that a simple reduction in the mean (background) cross-equatorial winds (Hu & Fedorov, 2018; Zhao & Fedorov, 2020) can provide a sufficient explanation of ENSO changes in the context of an AMOC slowdown under the background of anthropogenic warming.

We further probe the physical mechanisms by which a weakened AMOC modifies ENSO by utilizing the Bjerknes (BJ) stability index (Jin et al., 2006; Lu et al., 2019, 2016; Manucharyan & Fedorov, 2014; Zhao & Fedorov, 2020; Zhu et al., 2017), which allows us to evaluate quantitatively the role of ocean-atmosphere feedback and damping effects. The linear equation for temperature anomalies ( $T_o$ ) averaged within the mixed layer (i.e., the upper 50 m) in the tropical central and eastern equatorial Pacific (5°S–5°N, 180°E–80°W) can be written as:  $\partial T_o / \partial t = BJ * T_o + \dots$ , where the omitted terms describe the term proportional to the thermocline depth in the eastern Pacific (EP) and the system's noise, and

$$BJ = -\alpha_s - \alpha_{MA} + \mu_a \beta_a \langle -\bar{T}_x \rangle + \mu_a \beta_w \langle -\bar{T}_z \rangle + \mu_a \beta_h \left\langle \frac{\bar{w}}{H_1} \right\rangle a_h \quad (1)$$

TD      MA      ZA      EK      TH

From Equation 1, the BJ index is a sum of five feedback terms: (a) the net surface heat flux feedback, or thermodynamic damping (TD), (b) the mean advection feedback (MA), (c) the zonal advection feedback (ZA), (d): the Ekman upwelling feedback (EK) and (e) the thermocline feedback (TH). Terms (a) and (b) describe negative feedback processes that damp SST anomalies. Terms (c)–(e) denote positive feedback processes that



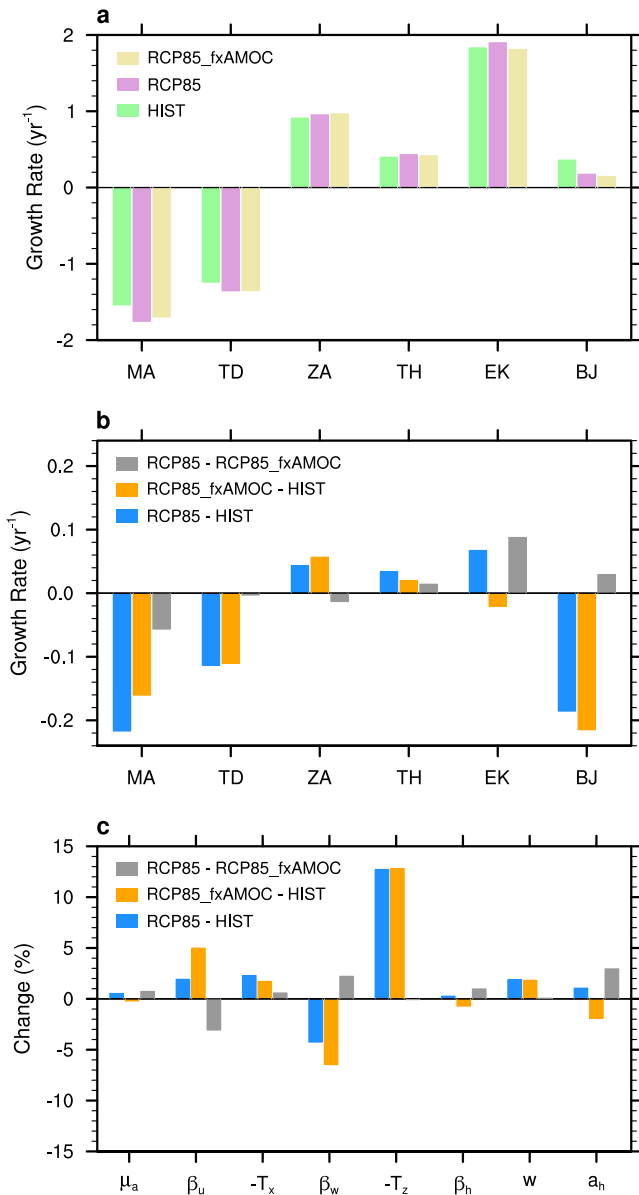


**Figure 3.** (a) The BJ index for the HIST (green), RCP85 (purple), and RCP85\_fxAMOC (yellow) simulations. MA, TD, ZA, TH, and EK represent the mean advection, thermal damping, zonal advection, thermocline, and Ekman feedback, respectively. The panel shows the ensemble-mean result. (b) Similar to panel (a) but for changes between simulations (RCP85 – HIST, blue; RCP85\_fxAMOC – HIST, orange; RCP85 – RCP85\_fxAMOC, gray). (c) Similar to panel (b) but for changes in the percentage of different regression coefficients and mean temperature gradients relative to HIST.

intensify SST anomalies. Together they represent the combined effects of the background state, including the mean zonal and vertical ocean temperature gradients and vertical ocean velocity ( $\bar{T}_x$ ,  $\bar{T}_z$ ,  $\bar{w}$ ), atmospheric (wind stress) response to SST anomalies ( $\mu_a$ ), and oceanic response to equatorial wind stress anomalies ( $\beta_w$ ,  $\beta_u$ , and  $\beta_h$ ) for thermocline slope, upwelling and zonal currents on the growth of ENSO SST anomalies.  $a_h$  denotes the sensitivity between ocean subsurface temperature and sea level anomalies.  $H_1$  denotes an effective depth for vertical advection.

We find that, consistent with the weakened ENSO variability from the HIST to RCP85 simulation, the total BJ index on average reduces by 51.6%. This reduction in the BJ index can be mostly attributed to stronger negative feedback, including the thermodynamic damping and mean advection feedback (Figures 3a and 3b). Moreover, if the AMOC stayed constant after the 1980s, the total BJ index would on average increase by 16.9%, which is consistent with the strengthening of ENSO variability from the RCP85\_fxAMOC to RCP85 simulation. This relative increase in the BJ index is mainly caused by stronger positive Ekman upwelling feedback (Figures 3a and 3b), which results from enhanced atmospheric wind stress response to SST anomalies ( $\mu_a$ ) and enhanced oceanic upwelling response to equatorial wind stress anomalies ( $\beta_w$ ) (Figure 3c). Note that while  $\beta_h$  and  $\mu_a$  have comparable percentage increases, the contribution from the thermocline feedback is small compared to that from the Ekman upwelling feedback.

Next, we investigate the impacts of AMOC slowdown on ENSO diversity, focusing on events characterized by the EP or CP patterns with maximum SST anomalies developing in the eastern and central Pacific, respectively (Ashok et al., 2007; Capotondi, 2013; Kao & Yu, 2009; Santos et al., 2019; Takahashi et al., 2011; Yu & Kao, 2007). To determine the type of particular El Niño events, we follow Takahashi et al. (2011) and first compute empirical orthogonal functions (EOFs) for the detrended monthly SST anomalies (relative to the SST climatology of the base period for each observation or model simulation) for the observations and for the HIST, RCP85, and RCP85\_fxAMOC simulations over a domain bounded by 10°S–10°N and the Pacific lateral boundaries. We focus on the first two principal components (PC1 and PC2), which are normalized by the standard deviation for the base period and smoothed with a 1-2-1 filter. The dimensional spatial SST patterns of EOF1 and EOF2 are then obtained by linearly regressing SST anomalies onto PC1 and PC2 (Figure S2 in Supporting Information S1).

Next, following Takahashi et al. (2011), we calculate the  $E$  and  $C$  indices for ENSO as follows:

$$E = \frac{PC1 - PC2}{\sqrt{2}} \quad (2)$$

$$C = \frac{PC1 + PC2}{\sqrt{2}} \quad (3)$$

These two indices describe the strength of EP and CP El Niño events, respectively. We linearly regress SST anomalies onto the  $E$  and  $C$  indices to obtain the dimensional spatial SST patterns corresponding to EP and CP El Niño events (Figure 4). The ensemble mean of observations for years 1861–1980 displays an EP pattern with maximum SST anomalies in the eastern equatorial Pacific and along the coast of Peru (Figure 4a) and a CP pattern with maximum SST anomalies over the central equatorial Pacific (Figure 4b). CCSM4 captures the general features of both EP and CP patterns seen in the observations during this period except with slightly large amplitudes of the EP pattern (Figure 4c) and a more westward maximum in the CP pattern (Figure 4d), which is similar to

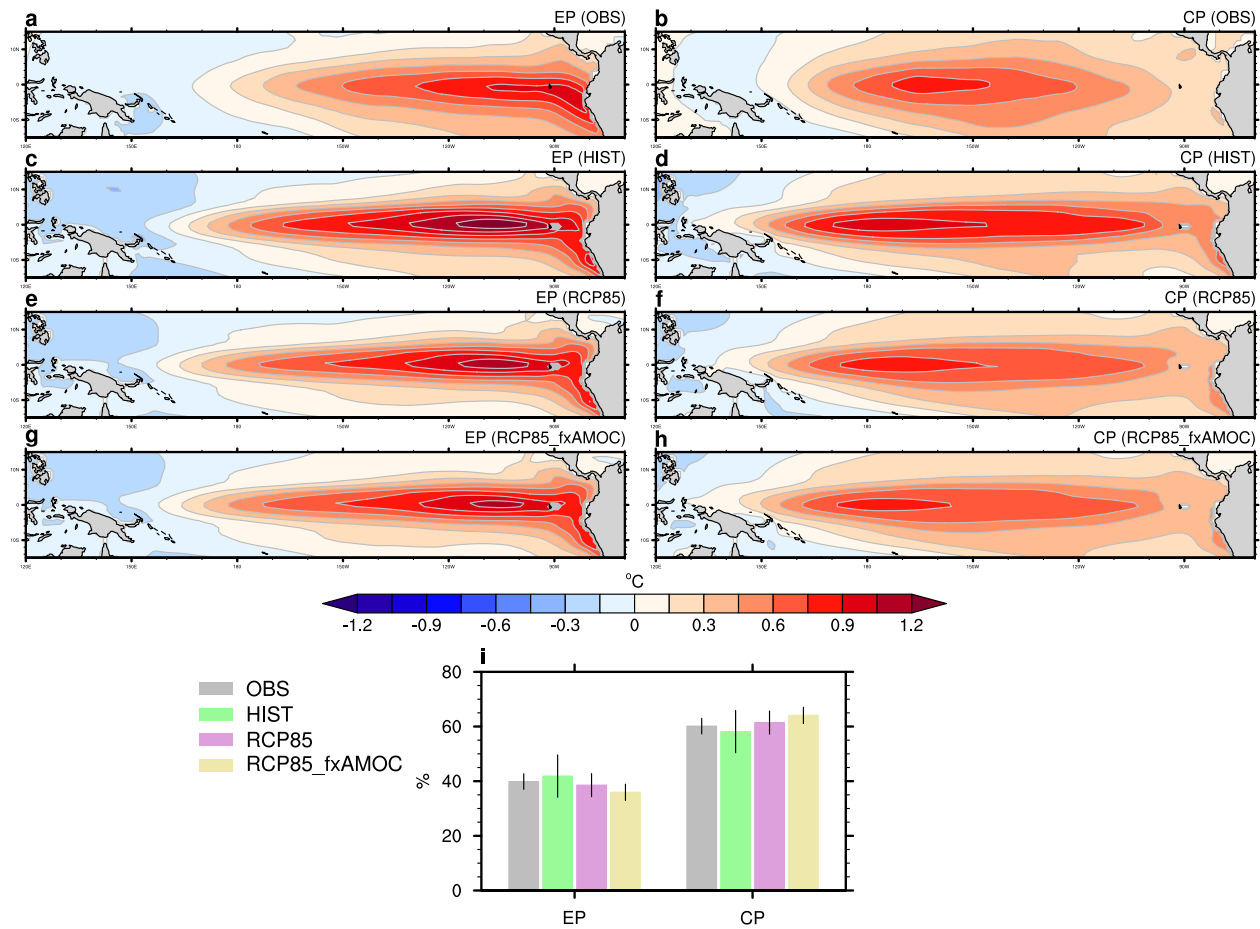


**Figure 4.** (a, c, e, g) Linear regression of sea surface temperature (SST) anomalies (color shading, in °C) onto the E-index for (a) observations, (c) the HIST simulation for years 1861–1980, and (e) RCP85 and (g) RCP85\_fxAMOC simulations, both for years 1981–2100. The panels show ensemble-mean results. (b, d, f, h) As in the left panels but for the SST regression onto the C-index. (i) The fraction of EP and CP El Niño events in the observations (gray), in the HIST simulation (green) for 1861–1980, and in the RCP85 (purple) and RCP85\_fxAMOC (yellow) simulations for 1981–2100. Bars denote one standard deviation.

other climate model simulations (Kim & Yu, 2012; Yu & Kim, 2010). During the twenty-first century, the SST anomaly maximum is projected to weaken for the EP pattern (Figure 4e) and to move westward for the CP pattern (Figure 4f) under the RCP8.5 scenario. Without the AMOC slowdown, the SST anomaly maximum would reduce even more for EP events (Figure 4g) and shift even more westward for CP events (Figure 4h).

We further employ the EP and CP indices to assess the frequency of El Niño events of different types. We define an EP or CP warm event when the corresponding averaged October–March index exceeds one standard deviation (Orihuela-Pinto et al., 2022). Observations show more CP than EP events (about three fifths vs. two fifths of the total number of warm events) between 1861 and 1980; the HIST simulation exhibits generally similar percentages of CP and EP events (Figure 4i). Since the 1980s, the RCP85 simulation suggests that CP El Niño events are more frequent than the EP events. If the AMOC did not weaken, the proportion of CP to EP ENSO events would on average further increase by 11.0% over 1981–2100 (Figure 4i), which is consistent with the result from Orihuela-Pinto et al. (2022). However, this AMOC impact of shifting El Niño events toward the CP type is statistically insignificant ( $p = 0.29$ ) relative to internal climate variability.

#### 4. Conclusion and Discussions

In this study, we isolate and quantify the AMOC impacts on ENSO in a warming climate using CCSM4 simulations. We find that the weakened AMOC causes a reduction in the SST annual cycle in the eastern equatorial Pacific and anomalous cross-equatorial northerly winds there, which leads to an increase in ENSO variance

by around 11% between 1981 and 2100 relative to the simulated ENSO weakening induced by anthropogenic warming. We further analyze the Bjerknes stability index and find that this ENSO intensification induced by the AMOC slowdown can be primarily attributed to the enhanced Ekman upwelling feedback related to amplified atmospheric response to SST anomalies as well as oceanic upwelling response to equatorial wind stress anomalies. We also find that the weakened AMOC modulates ENSO complexity by increasing the ratio of CP to EP events by approximately 11%. Nevertheless, both AMOC effects on ENSO magnitude and type are relatively small when compared to ENSO variations driven by internal climate variability.

It is noteworthy that the AMOC impacts on ENSO presented in our study are considered in the context of anthropogenic warming over the twenty-first century during which the AMOC will slow down but remain active, which are thus different from the impacts of a collapsed AMOC that is often considered in the paleoclimate context using idealized strong freshwater hosing experiments (Dong & Sutton, 2007; Orihuela-Pinto et al., 2022; Timmermann et al., 2007). It also merits attention that, compared to the AMOC modest impact on ENSO induced SST variance (Figure S3g in Supporting Information S1), the weakened overturning has a greater impact on inter-annual SST skewness and hence ENSO asymmetry (Figure S3h in Supporting Information S1). Over 1981–2100, the weakened AMOC generally reduces the ENSO skewness by decreasing positive SST skewness in the eastern Pacific and at the same time increasing negative skewness in the western Pacific. The maximum change in skewness can exceed 30% of its historical values (Figures S3b and S3h in Supporting Information S1).

We note that the simulated AMOC-induced changes in ENSO variability and the role of ocean-atmosphere feedback are opposite in our study and that of Orihuela-Pinto et al. (2022), which may reflect the delicate balance of amplifying and damping feedback in different model simulations. We also find significant differences in the AMOC-induced mean state changes in zonal winds and thermocline along the equatorial Pacific (Figure S4 in Supporting Information S1) between our study and Orihuela-Pinto et al. (2022), which to some extent reflects the model uncertainty as reported in Timmermann et al. (2007). Additionally, a recent study by Lee et al. (2021) has suggested that large ( $\geq 50$ ) ensembles are needed to robustly capture the baseline ENSO characteristics and physical processes. Given the large uncertainties in the IPCC AR5 model projections of ENSO intensity and the need of large ensembles, it would be important to apply the current framework to the state-of-art IPCC AR6 model large ensemble simulations to further tackle this scientific question.

## Data Availability Statement

COBE-SST2 data are publicly available at <https://ds.data.jma.go.jp/tcc/tcc/products/elnino/cobesst/cobe-sst.html>. ERSST.v4 & v5 data are publicly available at <https://www.ncei.noaa.gov/products/extended-reconstructed-sst>. KAPLAN EXTENDED v2 data are publicly available at <https://iridl.ldeo.columbia.edu/SOURCES/.KAPLAN/EXTENDED/.v2/.sst/datafiles.html?Set-Language=en>. The source code of CCSM4 is available at <https://www.cesm.ucar.edu/models/ccsm4.0/>. Model configuration parameters used to run the model experiment are available in W. Liu et al. (2020), <https://www.science.org/doi/10.1126/sciadv.aaz4876>. The data to generate Figures 1–4 are available at Zenodo DOI: <https://doi.org/10.5281/zenodo.7783335>.

## References

- An, S.-I., & Jin, F. F. (2000). An eigen analysis of the interdecadal changes in the structure and frequency of ENSO mode. *Geophysical Research Letters*, 27(16), 2573–2576. <https://doi.org/10.1029/1999gl011090>
- Ashok, K., Behera, S. K., Rao, S. A., Weng, H., & Yamagata, T. (2007). El Niño Modoki and its possible teleconnection. *Journal of Geophysical Research*, 112(C11), C11007. <https://doi.org/10.1029/2006jc003798>
- Bryden, H., & Imawaki, S. (2001). Ocean heat transport. Ocean circulation and climate. In G. Siedler, J. Church, & J. Gould (Eds.), *International Geophysics Series* (Vol. 77, pp. 317–336). Academic Press.
- Caesar, L., McCarthy, G. D., Thornalley, D. J. R., Cahill, N., & Rahmstorf, S. (2021). Current Atlantic Meridional Overturning Circulation weakest in last millennium. *Nature Geoscience*, 14(3), 118–120. <https://doi.org/10.1038/s41561-021-00699-z>
- Caesar, L., Rahmstorf, S., Robinson, A., Feulner, G., & Saba, W. (2018). Observed fingerprint of a weakening Atlantic Ocean overturning circulation. *Nature*, 556(7700), 191–196. <https://doi.org/10.1038/s41586-018-0006-5>
- Cai, W., Ng, B., Wang, G., Santoso, A., Wu, L., & Yang, K. (2022). Increased ENSO sea surface temperature variability under four IPCC emission scenarios. *Nature Climate Change*, 12(3), 228–231. <https://doi.org/10.1038/s41558-022-01282-z>
- Cai, W., Santoso, A., Wang, G., Yeh, S. W., Soon-Il, A., Cobb, K. M., et al. (2015). ENSO and greenhouse warming. *Nature Climate Change*, 5(9), 849–859. <https://doi.org/10.1038/nclimate2743>
- Capotondi, A. (2013). ENSO diversity in the NCAR CCSM4 climate model. *Journal of Geophysical Research: Oceans*, 118(10), 4755–4770. <https://doi.org/10.1002/jgrc.20335>
- Chang, P., Wang, B., Li, T., & Ji, L. (1994). Interactions between the seasonal cycle and the southern oscillation—Frequency entrainment and chaos in a coupled ocean-atmosphere model. *Geophysical Research Letters*, 21(25), 2817–2820. <https://doi.org/10.1029/94gl02759>

## Acknowledgments

This work is supported by grants to W.L. from U.S. National Science Foundation (AGS-2053121 and OCE-2123422). W.L. is also supported by the Hellman Fellows Fund as a Hellman Fellow. A.V.F. is supported by NSF (AGS-2053096), NOAA (NA20OAR4310377), DOE (DE-SC0023134), and by the ARCHANGE project of the “Make our planet great again” program (ANR-18-MPGA-0001, France). The CESM/CCSM4 project has been supported primarily by the National Science Foundation (NSF). This material is based upon work supported by the National Center for Atmospheric Research, which is a major facility sponsored by the NSF under Cooperative Agreement 1852977.



- Collins, M., An, S. I., Cai, W., Ganachaud, A., Guilyardi, E., Jin, F. F., et al. (2010). The impact of global warming on the tropical Pacific Ocean and El Niño. *Nature Geoscience*, 3(6), 391–397. <https://doi.org/10.1038/ngeo868>
- Delworth, T. L., & Dixon, K. W. (2006). Have anthropogenic aerosols delayed a greenhouse gas-induced weakening of the North Atlantic thermohaline circulation? *Geophysical Research Letters*, 33(2), L02606. <https://doi.org/10.1029/2005gl024980>
- Deser, C., Phillips, A. S., Tomas, R. A., Okumura, Y. M., Alexander, M. A., Capotondi, A., et al. (2012). ENSO and Pacific decadal variability in the Community Climate System Model version 4. *Journal of Climate*, 25(8), 2622–2651. <https://doi.org/10.1175/jcli-d-11-00301.1>
- Dong, B.-W., & Sutton, R. T. (2002). Adjustment of the coupled ocean-atmosphere system to a sudden change in the Thermohaline Circulation. *Geophysical Research Letters*, 29(15), L1728. <https://doi.org/10.1029/2002gl015229>
- Dong, B.-W., & Sutton, R. T. (2007). Enhancement of ENSO variability by a weakened Atlantic thermohaline circulation in a coupled GCM. *Journal of Climate*, 20(19), 4920–4939. <https://doi.org/10.1175/jcli4284.1>
- Fedorov, A. V., Hu, S., Wittenberg, A. T., Levine, A. F., & Deser, C. (2020). ENSO low-frequency modulation and mean state interactions. El Niño southern oscillation in a changing climate (pp. 173–198).
- Fedorov, A. V., & Philander, S. G. (2000). Is El Niño changing? *Science*, 288(5473), 1997–2002. <https://doi.org/10.1126/science.288.5473.1997>
- Fedorov, A. V., & Philander, S. G. (2001). A stability analysis of tropical ocean-atmosphere interactions: Bridging measurements and theory for El Niño. *Journal of Climate*, 14, 3086–3101. [https://doi.org/10.1175/1520-0442\(2001\)014<3086:asauto>2.0.co;2](https://doi.org/10.1175/1520-0442(2001)014<3086:asauto>2.0.co;2)
- Frajka-Williams, E. (2015). Estimating the Atlantic overturning at 26°N using satellite altimetry and cable measurements. *Geophysical Research Letters*, 42(9), 3458–3464. <https://doi.org/10.1002/2015gl063220>
- Hassan, T., Allen, R. J., Liu, W., & Randles, C. A. (2021). Anthropogenic aerosol forcing of the Atlantic meridional overturning circulation and the associated mechanisms in CMIP6 models. *Atmospheric Chemistry and Physics*, 21(8), 5821–5846. <https://doi.org/10.5194/acp-21-5821-2021>
- Heede, U. K., & Fedorov, A. V. (2021). Eastern equatorial Pacific warming delayed by aerosols and thermostat response to CO<sub>2</sub> increase. *Nature Climate Change*, 11(8), 696–703. <https://doi.org/10.1038/s41558-021-01101-x>
- Heede, U. K., & Fedorov, A. V. (2023). Colder eastern equatorial Pacific and stronger Walker circulation in the early 21st century: Separating the forced response to global warming from natural variability. *Geophysical Research Letters*, 50(3), e2022GL101020. <https://doi.org/10.1029/2022gl101020>
- Heede, U. K., Fedorov, A. V., & Burls, N. J. (2020). Time scales and mechanisms for the tropical Pacific response to global warming: A tug of war between the ocean thermostat and weaker walker. *Journal of Climate*, 33(14), 6101–6118. <https://doi.org/10.1175/jcli-d-19-0690.1>
- Heede, U. K., Fedorov, A. V., & Burls, N. J. (2021). A stronger versus weaker walker: Understanding model differences in fast and slow tropical Pacific responses to global warming. *Climate Dynamics*, 57(9–10), 2505–2522. <https://doi.org/10.1007/s00382-021-05818-5>
- Hirahara, S., Ishii, M., & Fukuda, Y. (2014). Centennial-scale sea surface temperature analysis and its uncertainty. *Journal of Climate*, 27(1), 57–75. <https://doi.org/10.1175/jcli-d-12-00837.1>
- Hu, S., & Fedorov, A. V. (2018). Cross-equatorial winds control El Niño diversity and change. *Nature Climate Change*, 8(9), 798–802. <https://doi.org/10.1038/s41558-018-0248-0>
- Huang, B., Banzon, V. F., Freeman, E., Lawrimore, J., Liu, W., Peterson, T. C., et al. (2015). Extended reconstructed sea surface temperature version 4 (ERSST.v4). Part I: Upgrades and intercomparisons. *Journal of Climate*, 28(3), 911–930. <https://doi.org/10.1175/jcli-d-14-00006.1>
- Huang, B., Thorne, P. W., Banzon, V. F., Boyer, T., Chepurin, G., Lawrimore, J. H., et al. (2017). Extended reconstructed sea surface temperature, version 5 (ERSST.v5): Upgrades, validations, and intercomparisons. *Journal of Climate*, 30(20), 8179–8205. <https://doi.org/10.1175/jcli-d-16-0836.1>
- IPCC. (2013). In T. F. Stocker, D. Qin, G. -K. Plattner, M. Tignor, S. K. Allen, J. Boschung, et al. (Eds.), *Climate change 2013: The physical science basis. Contribution of Working Group I to the Fifth Assessment Report of the Intergovernmental Panel on Climate Change* (p. 1535). Cambridge University Press.
- IPCC. (2021). In V. Masson-Delmotte, P. Zhai, A. Pirani, S. L. Connors, C. Péan, S. Berger, et al. (Eds.), *Climate change 2021: The physical science basis. Contribution of Working Group I to the Sixth Assessment Report of the Intergovernmental Panel on Climate Change* (p. 2391). Cambridge University Press.
- Jin, F.-F., Kim, S. T., & Bejarano, L. (2006). A coupled-stability index for ENSO. *Geophysical Research Letters*, 33(23), L23708. <https://doi.org/10.1029/2006gl027221>
- Kao, H.-Y., & Yu, J.-Y. (2009). Contrasting eastern-Pacific and central-Pacific types of ENSO. *Journal of Climate*, 22(3), 615–632. <https://doi.org/10.1175/2008jcli2309.1>
- Kaplan, A., Cane, M. A., Kushnir, Y., Clement, A. C., Blumenthal, M. B., & Rajagopalan, B. (1998). Analyses of global sea surface temperature 1856–1991. *Journal of Geophysical Research*, 103(C9), 18567–18589. <https://doi.org/10.1029/97jc01736>
- Kilbourne, K. H., Wanamaker, A. D., Moffa-Sanchez, P., Reynolds, D. J., Amrhein, D. E., Butler, P. G., et al. (2022). Atlantic circulation change still uncertain. *Nature Geoscience*, 15(3), 165–167. <https://doi.org/10.1038/s41561-022-00896-4>
- Kim, S. T., & Yu, J.-Y. (2012). The two types of ENSO in CMIP5 models. *Geophysical Research Letters*, 39(11), L11704. <https://doi.org/10.1029/2012gl052006>
- Knutson, T. R., & Manabe, S. (1995). Time-mean response over the tropical Pacific to increased CO<sub>2</sub> in a coupled ocean-atmosphere model. *Journal of Climate*, 8(9), 2181–2199. [https://doi.org/10.1175/1520-0442\(1995\)008<2181:tmrott>2.0.co;2](https://doi.org/10.1175/1520-0442(1995)008<2181:tmrott>2.0.co;2)
- Lee, J., Planton, Y. Y., Gleckler, P. J., Sperber, K. R., Guilyardi, E., Wittenberg, A. T., et al. (2021). Robust evaluation of ENSO in climate models: How many ensemble members are needed? *Geophysical Research Letters*, 48(20), e2021GL095041. <https://doi.org/10.1029/2021gl095041>
- Li, S., & Liu, W. (2022). Impacts of Arctic sea ice loss on global ocean circulations and interbasin ocean heat exchanges. *Climate Dynamics*, 59(9–10), 2701–2716. <https://doi.org/10.1007/s00382-022-06241-0>
- Liu, W., Fedorov, A. V., Xie, S.-P., & Hu, S. (2020). Climate impacts of a weakened Atlantic Meridional Overturning Circulation in a warming climate. *Science Advances*, 6(26), eaaz4876. <https://doi.org/10.1126/sciadv.aaz4876>
- Liu, W., Huang, B., Thorne, P. W., Banzon, V. F., Zhang, H. M., Freeman, E., et al. (2015). Extended Reconstructed Sea Surface Temperature version 4 (ERSST.v4). Part II: Parametric and structural uncertainty estimations. *Journal of Climate*, 28(3), 931–951. <https://doi.org/10.1175/jcli-d-14-00007.1>
- Liu, W., Xie, S.-P., Liu, Z., & Zhu, J. (2017). Overlooked possibility of a collapsed Atlantic Meridional Overturning Circulation in warming climate. *Science Advances*, 3(1), e1601666. <https://doi.org/10.1126/sciadv.1601666>
- Liu, Z. (2002). A simple model study of the forced response of ENSO to an external periodic forcing. *Journal of Climate*, 15(9), 1088–1098. [https://doi.org/10.1175/1520-0442\(2002\)015<1088:asmsoe>2.0.co;2](https://doi.org/10.1175/1520-0442(2002)015<1088:asmsoe>2.0.co;2)
- Liu, Z., Vavrus, S., He, F., Wen, N., & Zhong, Y. (2005). Rethinking tropical ocean response to global warming: The enhanced equatorial warming. *Journal of Climate*, 18(22), 4684–4700. <https://doi.org/10.1175/jcli3579.1>
- Lu, Z., Liu, Z., Chen, G., & Guan, J. (2019). Prominent precession band variance in ENSO intensity over the last 300,000 yr. *Geophysical Research Letters*, 46(16), 9786–9795. <https://doi.org/10.1029/2019gl083410>

- Lu, Z., Liu, Z., & Zhu, J. (2016). Abrupt intensification of ENSO forced by deglacial ice-sheet retreat in CCSM3. *Climate Dynamics*, 46(5–6), 1877–1891. <https://doi.org/10.1007/s00382-015-2681-3>
- Manucharyan, G. E., & Fedorov, A. V. (2014). Robust ENSO across a wide range of climates. *Journal of Climate*, 27(15), 5836–5850. <https://doi.org/10.1175/jcli-d-13-00759.1>
- Meehl, G. A., Collins, W. D., Boville, B. A., Kiehl, J. T., Wigley, T. M. L., & Arblaster, J. M. (2000). Response of the NCAR Climate System Model to increased CO<sub>2</sub> and the role of physical processes. *Journal of Climate*, 13(11), 1879–1898. [https://doi.org/10.1175/1520-0442\(2000\)013<1879:rotncs>2.0.co;2](https://doi.org/10.1175/1520-0442(2000)013<1879:rotncs>2.0.co;2)
- Menary, M. B., Robson, J., Allan, R. P., Booth, B. B. B., Cassou, C., Gastineau, G., et al. (2020). Aerosol-forced AMOC changes in CMIP6 historical simulations. *Geophysical Research Letters*, 47(14), e2020GL088166. <https://doi.org/10.1029/2020gl088166>
- Orihuela-Pinto, B., Santoso, A., England, M. H., & Taschetto, A. S. (2022). Reduced ENSO variability due to a collapsed Atlantic Meridional Overturning Circulation. *Journal of Climate*, 35(16), 5307–5320. <https://doi.org/10.1175/jcli-d-21-0293.1>
- Rahmstorf, S., Box, J. E., Feulner, G., Mann, M. E., Robinson, A., Rutherford, S., & Schaffernicht, E. J. (2015). Exceptional twentieth-century slowdown in Atlantic Ocean overturning circulation. *Nature Climate Change*, 5, 475–480. <https://doi.org/10.1038/nclimate2554>
- Ren, X., & Liu, W. (2021). The role of a weakened Atlantic meridional overturning circulation in modulating marine heatwaves in a warming climate. *Geophysical Research Letters*, 48(23), e2021GL095941. <https://doi.org/10.1029/2021gl095941>
- Roberts, C. D., Jackson, L., & McNeall, D. (2014). Is the 2004–2012 reduction of the Atlantic meridional overturning circulation significant? *Geophysical Research Letters*, 41(9), 3204–3210. <https://doi.org/10.1002/2014gl059473>
- Santoso, A., Hendon, H., Watkins, A., Power, S., Dommenges, D., England, M. H., et al. (2019). Dynamics and predictability of El Niño–Southern Oscillation: An Australian perspective on progress and challenges. *Bulletin of the American Meteorological Society*, 100(3), 403–420. <https://doi.org/10.1175/bams-d-18-0057.1>
- Smeed, D. A., Josey, S. A., Beaulieu, C., Johns, W. E., Moat, B. I., Frajka-Williams, E., et al. (2018). The North Atlantic Ocean is in a state of reduced overturning. *Geophysical Research Letters*, 45(3), 1527–1533. <https://doi.org/10.1002/2017gl076350>
- Stevenson, S. L. (2012). Significant changes to ENSO strength and impacts in the twenty-first century: Results from CMIP5. *Geophysical Research Letters*, 39(17), L17703. <https://doi.org/10.1029/2012gl052759>
- Takahashi, K., Montecinos, A., Goubanova, K., & Dewitte, B. (2011). ENSO regimes: Reinterpreting the canonical and Modoki El Niño. *Geophysical Research Letters*, 38(10), L10704. <https://doi.org/10.1029/2011gl047364>
- Thornalley, D. J. R., Oppo, D. W., Ortega, P., Robson, J. I., Brierley, C. M., Davis, R., et al. (2018). Anomalously weak Labrador Sea convection and Atlantic overturning during the past 150 yr. *Nature*, 556(7700), 227–230. <https://doi.org/10.1038/s41586-018-0007-4>
- Timmermann, A., Lorenz, S., An, S.-I., Clement, A., & Xie, S.-P. (2007). The effect of orbital forcing on the mean climate and variability of the tropical Pacific. *Journal of Climate*, 20(16), 4147–4159. <https://doi.org/10.1175/jcli4240.1>
- Timmermann, A., Okumura, Y., An, S. I., Clement, A., Dong, B., Guilyardi, E., et al. (2007). The influence of a weakening of the Atlantic meridional overturning circulation on ENSO. *Journal of Climate*, 20(19), 4899–4919. <https://doi.org/10.1175/jcli4283.1>
- Weijer, W., Cheng, W., Garuba, O. A., Hu, A., & Nadiga, B. T. (2020). CMIP6 models predict significant 21st century decline of the Atlantic Meridional Overturning Circulation. *Geophysical Research Letters*, 47(12), e2019GL086075. <https://doi.org/10.1029/2019gl086075>
- Williamson, M. S., Collins, M., Drijfhout, S. S., Kahana, R., Mecking, J. V., & Lenton, T. M. (2018). Effect of AMOC collapse on ENSO in a high-resolution general circulation model. *Climate Dynamics*, 50(7–8), 2537–2552. <https://doi.org/10.1007/s00382-017-3756-0>
- Xie, S.-P., Deser, C., Vecchi, G. A., Ma, J., Teng, H., & Wittenberg, A. T. (2010). Global warming pattern formation: Sea surface temperature and rainfall. *Journal of Climate*, 23(4), 966–986. <https://doi.org/10.1175/2009jcli3329.1>
- Xie, S.-P., & Philander, S. G. H. (1994). A coupled ocean-atmosphere model of relevance to the ITCZ in the eastern Pacific. *Tellus*, 46A(4), 340–350. <https://doi.org/10.1034/j.1600-0870.1994.t01-1-00001.x>
- Yu, J.-Y., & Kao, H.-Y. (2007). Decadal changes of ENSO persistence barrier in SST and ocean heat content indices: 1958–2001. *Journal of Geophysical Research: Atmospheres*, 112(D13), D13106. <https://doi.org/10.1029/2006jd007654>
- Yu, J.-Y., & Kim, S. T. (2010). Identification of central-Pacific and eastern-Pacific types of ENSO in CMIP3 models. *Geophysical Research Letters*, 37(15), L15705. <https://doi.org/10.1029/2010gl044082>
- Zhang, R., & Delworth, T. (2005). Simulated tropical response to a substantial weakening of the Atlantic thermohaline circulation. *Journal of Climate*, 18(12), 1853–1860. <https://doi.org/10.1175/jcli3460.1>
- Zhao, B., & Fedorov, A. V. (2020). The effects of background zonal and meridional winds on ENSO in a coupled GCM. *Journal of Climate*, 33(6), 2075–2091. <https://doi.org/10.1175/jcli-d-18-0822.1>
- Zheng, X.-T., Hui, C., & Yeh, S. W. (2019). Response of ENSO amplitude to global warming in CESM large ensemble: Uncertainty due to internal variability. *Climate Dynamics*, 50(11–12), 4019–4035. <https://doi.org/10.1007/s00382-017-3859-7>
- Zheng, X.-T., Xie, S.-P., Lv, L.-H., & Zhou, Z.-Q. (2016). Intermodel uncertainty in ENSO amplitude change tied to Pacific Ocean warming pattern. *Journal of Climate*, 29(20), 7265–7279. <https://doi.org/10.1175/jcli-d-16-0039.1>
- Zhu, J., Liu, Z., Brady, E., Otto-Bliesner, B., Zhang, J., Noone, D., et al. (2017). Reduced ENSO variability at the LGM revealed by an isotope-enabled Earth system model. *Geophysical Research Letters*, 44(13), 6984–6992. <https://doi.org/10.1002/2017gl073406>